

Fixes That Fail: Self-Defeating Improvements in Machine-Learning Systems

Ruihan Wu¹ Chuan Guo² Awni Hannun² Laurens van der Maaten²

Abstract

Machine-learning systems such as self-driving cars or virtual assistants are composed of a large number of machine-learning models that recognize image content, transcribe speech, analyze natural language, infer preferences, rank options, *etc.* These systems can be represented as directed acyclic graphs in which each vertex is a model, and models feed each other information over the edges. Oftentimes, the models are developed and trained independently, which raises an obvious concern: *Can improving a machine-learning model make the overall system worse?* We answer this question affirmatively by showing that improving a model can deteriorate the performance of downstream models, even after those downstream models are retrained. Such *self-defeating improvements* are the result of entanglement between the models. We identify different types of entanglement and demonstrate via simple experiments how they can produce self-defeating improvements. We also show that self-defeating improvements emerge in a realistic stereo-based object detection system.

The first rule of systems engineering is: If you optimize the components you will probably ruin the system performance.

Richard Hamming

1. Introduction

Progress in machine learning has allowed us to develop increasingly complex artificially intelligent systems, including self-driving cars, virtual assistants, and complex robots. These systems generally contain a large number of machine-learning models that are trained to perform tasks such as recognizing image or video content, transcribing

speech, analyzing natural language, eliciting user preferences, ranking options to be presented to a user, *etc.* The models feed each other information: for example, a pedestrian detector may use the output of a depth-estimation model as input. Indeed, machine-learning systems can be interpreted as directed acyclic graphs in which each vertex corresponds to a model, and models feed each other information over the edges in the graph. In practice, the models in the graph are often developed and trained independently (Nushi et al., 2017). This modularization tends to lead to more usable APIs but may also be motivated by other practical constraints. For example, some of the models in the system may be developed by different teams (some models in the system may be developed by a cloud provider); models may be retrained and deployed at a very different cadence (personalization models may be updated very regularly but image-recognition models may not); new downstream models may be added continuously in the graph (user-specific models may need to be created every time a user signs up for a service); or models may be non-differentiable (gradient-boosted decision trees are commonly used for selection of discrete features). This can make backpropagation through the models in the graph infeasible or highly undesirable in many practical settings.

The scenario described above leads to an obvious potential concern: *Can improving a machine-learning model make the machine-learning system worse?* This study answers this question affirmatively by showing that improving an upstream model can deteriorate the performance of downstream models, *even if all the downstream models are retrained* after the update of the upstream model. Such *self-defeating improvements* are caused by entanglement between the models in the system. Our study identifies different types of entanglement, and presents experiments with synthetic systems that demonstrate how these entanglement types can lead to self-defeating improvements. We also show that self-defeating improvements arise in a realistic system that detects cars and pedestrians in stereo images.

Our study opens up a plethora of new research problems that, hitherto, have not been studied in-depth in the machine-learning community. We hope that our study will encourage the community to move beyond the study of machine-learning models in isolation, and to study machine-learning systems more holistically instead.

Work performed during internship at Facebook AI Research.
¹Cornell University ²Facebook AI Research. Correspondence to: Ruihan Wu <rw565@cornell.edu>, Laurens van der Maaten <lvdmaaten@fb.com>.

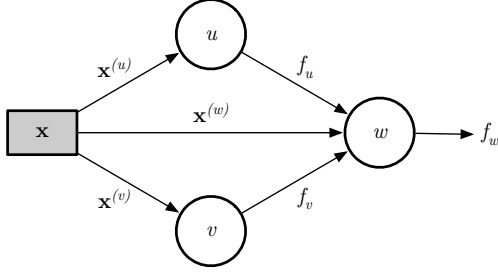


Figure 1. Example of a machine-learning system with three models, $\mathcal{V} = \{u, v, w\}$, and two edges, $\mathcal{E} = \{(u, w), (v, w)\}$. The system receives an example \mathbf{x} as input, of which parts $\mathbf{x}^{(u)}$, $\mathbf{x}^{(v)}$, and $\mathbf{x}^{(w)}$ are fed into u , v , and w , respectively. Model w 's input is concatenated with the outputs of its parents, $f_u(\mathbf{x})$ and $f_v(\mathbf{x})$.

2. Problem Setting

We model a machine-learning system as a static directed acyclic graph (DAG) of machine-learning models, $G = (\mathcal{V}, \mathcal{E})$, where each vertex $v \in \mathcal{V}$ corresponds to a machine-learning model and each edge $(v, w) \in \mathcal{E}$ represents the output of model v being used as input into model w . For example, vertex v could be a depth-estimation model and vertex w a pedestrian-detection model that operates on the depth estimates produced by vertex v . A model is *upstream* of v if it is an ancestor of v . A *downstream* model of v is a descendent of v . An example of a machine-learning system with three models is shown in Figure 1.

Each vertex in the machine-learning system G corresponds to a model function, $v(\cdot)$, that operates on both data and outputs from its upstream models. Denote the output from model v by $f_v(\mathbf{x})$. The output of a source model v is $f_v(\mathbf{x}) = v(\mathbf{x}^{(v)})$, where $\mathbf{x}^{(v)}$ represents the part of input \mathbf{x} that is relevant to model v . The output of a non-source model v is given by $f_v(\mathbf{x}) = v([\mathbf{x}^{(v)}, f_w(\mathbf{x})] : w \in \mathcal{P}_v]$, where $\mathcal{P}_v = \{w : (w, v) \in \mathcal{E}\}$ are the parents of model v .

Training. To train model v , we assume access to a training set $\mathcal{D}_v = \{(\mathbf{x}_1, \mathbf{y}_1), \dots, (\mathbf{x}_N, \mathbf{y}_N)\}$ with N_v examples $\mathbf{x}_n \in \mathcal{X}$ and corresponding targets $\mathbf{y}_n \in \mathcal{Y}_v$. For each model, we also assume a training algorithm $A_v(\mathcal{D}_v)$ that selects a model $v \in \mathcal{H}_v$ from hypothesis set \mathcal{H}_v based on the training set. The learning algorithm, A_v , the hypothesis set, \mathcal{H}_v , and the training set, \mathcal{D}_v , are fixed during training but they may change each time model v is re-trained or updated. The data space \mathcal{X} , the target space \mathcal{Y}_v , and the way in which inputs $\mathbf{x}^{(v)}$ are obtained from \mathbf{x} are fixed.

We assume that models v may be trained *separately* rather than jointly, that is, the learning signal obtained from training a downstream model, v , may not be backpropagated into its upstream dependencies, $w \in \mathcal{P}_v$ (see motivation below). Note that this implies that a downstream model cannot be trained before all its upstream models are trained.

Evaluation. To be able to evaluate the performance of the task at v , we assume access to a *fixed* test set $\bar{\mathcal{D}}_v$ that is defined analogously to the training set: it contains M_v test examples $\bar{\mathbf{x}}_m \in \mathcal{X}$ and corresponding targets $\bar{\mathbf{y}}_m \in \mathcal{Y}_v$. In contrast to the training set, the test set is fixed and does not change when the model is updated. However, we note that the input distribution into a non-root model is not only governed by the test set $\bar{\mathcal{D}}_v$ but also by upstream models: if an upstream model changes, the inputs into a downstream model may change as well even though the test set is fixed.

We also assume access to a *test loss* function $\ell_v(v, \bar{\mathcal{D}}_v)$ for each model v , for example, classification error (we assume lower is better). Akin to the test set $\bar{\mathcal{D}}_v$, all test loss functions ℓ_v are fixed. Hence, we always measure the generalization ability of a model, v , in the exact same way. The test loss function may not have trainable parameters.

Updating models. The machine-learning system we defined can be improved by updating a model. In such an update, an individual model v is replaced by an alternative model v' . We can determine if such a model update constitutes an *improvement* by evaluating whether or not its test loss decreases: $\ell_v(v, \bar{\mathcal{D}}_v) \leq \ell_v(v', \bar{\mathcal{D}}_v)$. When v is not a leaf in G , the update to v' may affect the test loss of downstream models as well. In practice, the improvement due to v' often also improves downstream models (e.g., Kornblith et al. (2019)), but this is not guaranteed. We define a *self-defeating improvement* as a situation in which replacing v by v' improves that model but deteriorates at least one of the downstream models w , even after all the downstream models are updated (i.e., re-trained using the same learning algorithm) to account for the changes incurred by v' .

Definition 2.1 (Self-defeating improvement). Denoting the set of all downstream models (descendants) of v in G as \mathcal{C}_v , a *self-defeating improvement* arises when:

$$\exists w \in \mathcal{C}_v : \ell_v(v', \bar{\mathcal{D}}_v) \leq \ell_v(v, \bar{\mathcal{D}}_v) \not\Rightarrow \ell_w(w', \bar{\mathcal{D}}_w) \leq \ell_w(w, \bar{\mathcal{D}}_w),$$

where w' represents a new version of model w that was trained after model v was updated to v' to account for the input distribution change that the update of v incurs on w .

Motivation of problem setting. In the problem setting described above, we have made two assumptions: (1) models may be (re-)trained separately rather than jointly and (2) the training algorithm, hypothesis set, and training data may change between updates of the model¹. Both assumptions are motivated by the practice of developing large machine-learning systems that may comprise thousands of models (Nushi et al., 2017; Sculley et al., 2015). Joint model training is often infeasible in such systems because:

¹The training data does not change during training, i.e., we do not consider online learning settings in this study.

- Some of the models may have been developed by cloud providers, as a result of which they cannot be changed.
- Backpropagation may be technically infeasible or inefficient, for example, when some models are implemented in incompatible learning frameworks or when their respective training data lives in different data centers.
- Some models may be re-trained or updated more often than others. For example, personalization models may be updated every few hours to adapt to changes in the data distribution, but re-training large language models (Brown et al., 2020) at that cadence is impractical.
- Upstream models may have hundreds or even thousands of downstream dependencies, complicating appropriate weighting of the downstream learning signals that multi-task learning (Caruana, 1997) requires.
- Some models may be non-differentiable, for example, gradient-boosted decision trees are commonly used for feature selection in large sets of features.

We assume that changes in the training algorithm, hypothesis set, and training data may occur because model owners (for example, cloud providers) constantly seek to train and deploy improved versions of their models.

3. How Self-Defeating Improvements Arise

Traditional software design relies heavily on *modules*: independent and interchangeable components that are combined to form complex software systems (Glenn Brooks-hear, 2009, §7.4). Well-designed modules can be modified independently without affecting other modules in the system. As a result, improvements to a module (e.g., to its efficiency) generally improve the entire system. Ideally, the machine-learning models in the system from Section 2 would behave akin to traditional software modules. If they did, improving any model would improve the entire system.

However, machine-learned models rarely behave like modules in practice because they lack an explicit specification of their functionality (D’Amour et al., 2020). As a result, there is often a significant degree of *entanglement* between different models in the system (Nushi et al., 2017). We will demonstrate that this entanglement can lead to self-defeating improvements. On a high level, we separate entanglements into two main categories: (1) entanglement between an upstream model and its downstream dependency, and (2) entanglement between multiple upstream models that affects the downstream dependency.

3.1. Upstream-Downstream Entanglement

We can understand entanglement between an upstream model and its downstream dependency in a simple system that has two vertices, $\mathcal{V} = \{v, w\}$, and a dependency between upstream model v and downstream model w , that is,

$\mathcal{E} = \{(v, w)\}$. Entanglement in this system can lead to self-defeating improvements when there is a mismatch between the test loss of models v and w . We identify three types of mismatches: (1) loss-function mismatch, (2) data-distribution mismatch, and (3) hypothesis-space mismatch.

Loss-function mismatch refers to settings in which the test loss functions, ℓ , of the upstream and downstream model optimize for different things. For example, the upstream test loss function may not penalize certain types of errors that need to be avoided in order for the downstream test loss to be minimized, and it may penalize other types of errors that are irrelevant to the downstream model. This mismatch can lead to self-defeating improvements: the upstream model may be improved (per its test loss function) despite making more errors that negatively affect the downstream model. This may deteriorate the downstream test loss even after the downstream model is re-trained.

Data-distribution mismatch refers to settings in which the upstream loss focuses on parts of the data-target space $\mathcal{X} \times \mathcal{Y}_v$ that are unimportant for the downstream model (and vice versa). For example, suppose the upstream model v is an image-recognition model that aims to learn a feature representation that separates cats from dogs, and $f_v(\mathbf{x})$ is a feature representation obtained from that model. Then a downstream model, w , that aims to distinguish different dog breeds based on f_v may suffer from self-defeating improvements (e.g., Kornblith et al. (2019)). Specifically, model v can be improved by collapsing all representations corresponding to a dog image onto a single point, but this will make it impossible for model w to perform better than random (even after re-training). Data-distribution mismatch is related to domain adaptation, but it is more general because v ’s input data space may differ from that of w (domain adaptation assumes both data spaces to be the same).

Hypothesis-space mismatch arises when the downstream model, w , is unable to exploit improvements in the upstream model, v , because exploiting those improvements would require selection of a model that is not in the hypothesis space \mathcal{H}_w . Figure 2 illustrates how hypothesis-space mismatch can lead to self-defeating improvements. The upstream model, v , predicts a 2D position for each example (represented by shapes). The downstream model, w , separates examples into two classes (represented by colors) based on the prediction of v using a linear classifier. The predictions of the improved upstream model, v' , better match the ground-truth targets. However, the re-trained downstream model, w' , deteriorates because the resulting classification problem has become more non-linear.

3.2. Upstream-Upstream Entanglement

More complex types of self-defeating improvements may arise when a downstream model depends on multiple up-

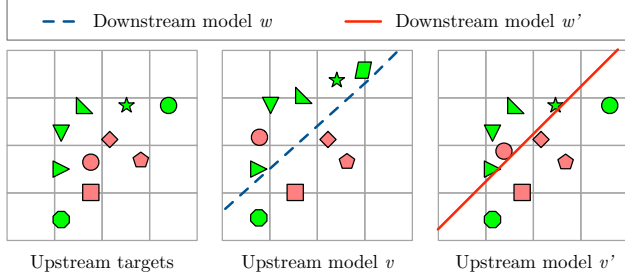


Figure 2. Illustration of a self-defeating improvement due to hypothesis-space mismatch. Upstream model v predicts a 2D point for each example (shape). Downstream model w is a linear classifier separating the points into two classes (red and green). **Left:** Ground-truth targets for the upstream model. **Middle:** Point predictions by upstream model v and the classifier learned by downstream model w . **Right:** Point predictions by improved upstream model v' and the corresponding downstream classifier w' . Note how the predictions of v' better match the ground-truth, but w' cannot exploit the improvement because it is linear.

stream models that are themselves entangled. Consider the system of Figure 1 that has three models, $\mathcal{V} = \{u, v, w\}$, and dependencies between upstream models u and v and downstream model w , that is, $\mathcal{E} = \{(u, w), (v, w)\}$. Self-defeating improvements can arise in this system, for example, when upstream models u and v make **anti-correlated errors** that cancel each other out. If v is improved by replacing it with a perfect v' , this exposes the errors made by u in a way that downstream model w cannot recover from.

We illustrate this type of self-defeating improvement in Figure 3. In the example, all three models aim to distinguish two classes: green (positive class) and red (negative class). Upstream models u and v do so based the (x, y) -location of points in the 2D plane. The downstream model operates on the (hard) outputs of the two upstream models. The original upstream models u and v make errors that are anti-correlated. The original downstream model w exploits this anti-correlation to make perfect predictions. When upstream model u is replaced by an improved model u' that makes no errors, a self-defeating improvement arises: downstream model w no longer receives the information it needs to separate both classes perfectly.

While the example in Figure 3 may seem contrived, anti-correlated errors can arise in practice when there are dependencies in the targets used to train different models. For example, suppose the upstream models are trained to predict ad clicks (*will a user click on an ad?*) and ad conversions (*will a user purchase the product being advertised?*), respectively. Because conversion can only happen after a click happens, there are strong dependencies between the targets used to train both models. As a result, a small set of mislabeled training examples in the targets for one of the upstream models can introduce anti-correlated errors.

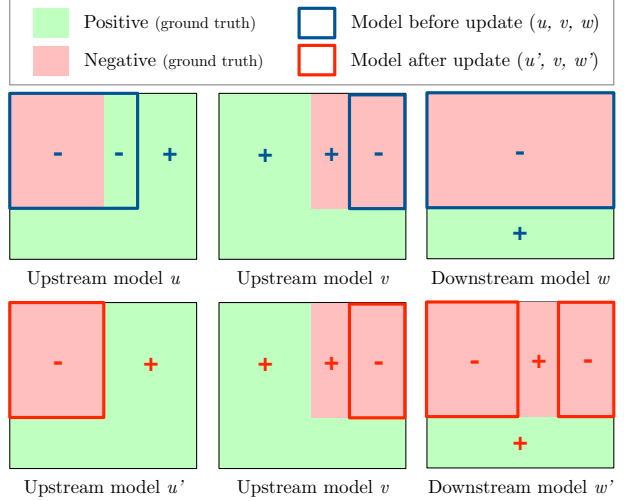


Figure 3. Illustration of self-defeating improvement due to anti-correlated errors. Green areas should be labeled as positive; red areas as negative. **Left:** Original upstream model u (top; blue line and +, - symbols) and its improved version u' (bottom; red). **Middle:** Upstream model v . **Right:** Original downstream model w (top) and its re-trained version w' (bottom). The errors of u and v are anti-correlated. As a result, the improved upstream model u' negatively impacts the re-trained downstream model w' .

4. Examples of Self-Defeating Improvements

To study how entanglement can lead to self-defeating improvements, we experiment on the Street View House Numbers (SVHN; Netzer et al. (2011)) dataset, which contains digit images with 10 classes. We group our experiments by entanglement type; see Table 1 for an overview. We repeat each experiment 40 times and report average performance and standard deviation across runs. Code is available at https://github.com/facebookresearch/self_defeating_improvements.

4.1. Upstream-Downstream Entanglement

We perform experiments to study how different types of upstream-downstream entanglement can lead to self-defeating improvements. We assume an upstream model, v , that provides inputs to a downstream model, w .

4.1.1. LOSS-FUNCTION MISMATCH

Our first experiment focuses on loss-function mismatch.

Upstream model. The basis of our upstream model is a ResNet-18 (He et al., 2016). We train the model to regress onto real-valued class numbers 1, 3, 7, and 9 by minimizing a mean squared error (MSE) on the model prediction, $v(\mathbf{x})$. The upstream test loss function, ℓ_v , is also MSE. To vary the performance of the upstream model, we add additional training examples with noisy labels to the training set, \mathcal{D}_v .

Fixes That Fail: Self-Defeating Improvements in Machine-Learning Systems

Scenario		Task	Training set (\mathcal{D})	Hypotheses (\mathcal{H})	Output (f)	Loss function (ℓ)
Loss-function mismatch (4.1.1)	Upstream (v)	Regress on 1, 3, 7 and 9	Noisy labels (1 : r)	ResNet-18	Outcome	Mean squared error
	Downstream (w)	1 vs. 3 vs. 7 vs. 9	Regular	MLP	Class label	Zero-one loss
Data-distribution mismatch (4.1.2)	Upstream (v)	$\{0, 1, 4, 7, 9\}$ vs. $\{2, 3, 5, 6, 8\}$	Subset ($p\%$)	ResNet-18	Features	Nearest neighbor
	Downstream (w)	1 vs. 7	Regular	Linear	Class label	Zero-one loss
Hypothesis-space mismatch (4.1.3)	Upstream (v)	Ten-class classification	Regular	Conv. network	Features	Nearest neighbor
	Downstream (w)	Ten-class classification	Regular	Linear	Class label	Zero-one loss
Anti-correlated errors (4.2)	Upstream (u, v)	Upstream u : $\{1, 6\}$ vs. 7 Upstream v : 1 vs. $\{6, 7\}$	Noisy labels ($p\%$)	ResNet-18	Class label	Zero-one loss
	Downstream (w)	$\{1, 7\}$ vs. 6	Regular	Bayes-optimal	Class label	Zero-one loss

Table 1. Overview of the settings of our experiments on the SVHN dataset, investigating how different types of entanglement (rows) can lead to self-defeating improvements. See text for detailed descriptions of each of the experiments.

The label noise flips the labels 1 and 3 with probability $1/2$, and flips labels 7 and 9 with probability $1/2$. We denote the ratio between the (fixed) number of clean examples and the number of additional noisy examples in the training set by $1 : r$. The test dataset, \mathcal{D}_v , is fixed and has clean labels.

Downstream model. The downstream model, w , receives the real-valued digit prediction, $v(\mathbf{x})$. It is a logistic regressor with one hidden layer (with 128 hidden units) trained to separate classes 1, 3, 7 and 9 based on the value $v(\mathbf{x})$. The downstream test loss function, ℓ_w , is the zero-one loss, that is, we measure the model’s classification error.

Results. Figure 4(a) shows the test loss of the upstream model (MSE) and downstream model (zero-one loss) as a function of the proportion of additional noisy training examples, r , in the training set. Even though their labels are noisy, the additional training examples improve the performance of the upstream model. The label noise does not affect the upstream model much, because confusing 1 and 3 or 7 and 9 is relatively harmless in terms of the MSE loss. However, the performance of the downstream model does deteriorate as a function of r . This deterioration occurs because the improved upstream model provides less signal on the differences between 1 and 3 and between 7 and 9, respectively. These are exactly the differences that need to be modeled accurately for the downstream model to perform well. Hence, this example illustrates how loss mismatch can lead to a self-defeating improvement.

4.1.2. DATA-DISTRIBUTION MISMATCH

Next, we study data-distribution mismatch.

Upstream model. The basis of our upstream model is a ResNet-18 (He et al., 2016) that is trained to distinguish classes $\{0, 1, 4, 7, 9\}$ from classes $\{2, 3, 5, 6, 8\}$. The upstream model, v , is the feature-producing network without the final linear layer. The upstream test loss function, ℓ_v , is the nearest neighbor error of predicting the right class based on $v(\mathbf{x})$. To alter the performance of v , we train models on $p=10\%$ to $p=100\%$ of the training set.

Downstream model. The downstream model w is a linear logistic regressor that is trained to separate classes 1 and 7 based on $v(\mathbf{x})$. As before, the corresponding downstream test loss function, ℓ_w , is the zero-one loss.

Results. Figure 4(b) shows the test loss of the upstream and downstream model as a function of the subsample ratio, p , of the upstream training set. As expected, the upstream loss (blue line) decreases with more training data. However, the downstream loss (orange line) deteriorates as the upstream model improves. This self-defeating improvement occurs because the upstream model benefits from collapsing classes 1 and 7, whereas the downstream model seeks to distinguish those classes. As the number of training examples increases, the upstream model gets better at collapsing the two classes, which deteriorates the downstream loss.

We also observe that the downstream loss has high standard deviation. We hypothesize this is due to the upstream model being *underspecified* (D’Amour et al., 2020): while collapsing classes 1 and 7 is sufficient for the upstream model to obtain perfect performance, collapsing may not be necessary. This underspecification may cause upstream outputs to vary substantially between training runs, leading to variations in the performance of the downstream model.

4.1.3. HYPOTHESIS-SPACE MISMATCH

We also experiment with hypothesis-space mismatch.

Upstream model. The upstream model, v , is a small feature-producing convolutional network. The network is trained to perform 10-class classification via a multi-layer perceptron (MLP) on top that minimizes multi-class logistic loss. As before, the test loss function, ℓ_v , is the nearest neighbor error of the extracted features. To vary v ’s performance, we vary the number of hidden layers in the MLP.

Downstream model. The downstream model, w , also performs 10-class classification but it is a linear logistic regressor that takes the features $v(\mathbf{x})$ as input. Again, the corresponding test loss function, ℓ_w , is the zero-one loss.

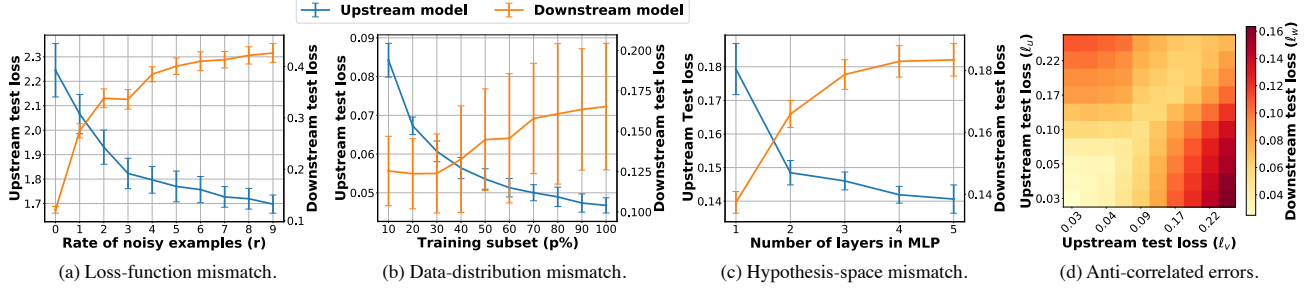


Figure 4. Examples of self-defeating improvements for each entanglement type on various instantiations of the SVHN dataset: (a) results of loss-function mismatch experiments in 4.1.1; (b) results of data-distribution mismatch experiments in 4.1.2; (c) results of hypothesis-space mismatch experiments in 4.1.3; and (d) results of anti-correlated errors experiments in 4.2. See Table 1 and text for details.

Results. Figure 4(c) plots the upstream and downstream test loss as a function of the number of layers in the MLP. For the upstream model, increasing the depth of fully-connected layers allows the convolutional layers to produce features that are more discriminative between classes. As a result, the features are tightly clustered by class, which translates to a monotonic decrease in the upstream test loss (blue line). However, the downstream model is unable to take advantage of the improved representation produced by v due to its limited hypothesis space. As a result, the improvement of the upstream model leads to a higher downstream test loss (orange line). Increasing the size of the downstream hypothesis space, \mathcal{H}_w , is likely to resolve this self-defeating improvement.

4.2. Upstream-Upstream Entanglement

We study how **anti-correlated errors** between two upstream models can lead to self-defeating improvements.

Upstream models. We consider two upstream models u and v that solve binary classification problems $\{1, 6\}$ versus 7 and 1 versus $\{6, 7\}$, respectively. Both the training and test set are balanced across the three classes (note that this implies the binary classification problems are unbalanced). We vary the performance of the upstream model by introducing label noise on classes 1 and 7 in the training set. Specifically, we follow Arazo et al. (2019) and rank all training examples in decreasing order of difficulty based on the area under the training-loss curve of the example. Next, we flip the label of the $p\%$ highest-ranked examples with classes 1 and 7, changing 1 to 7 and 7 to 1. The upstream test losses, ℓ_u and ℓ_v , are the zero-one loss.

Downstream model. The downstream model, w , receives binary class predictions from u and v and tries to distinguish between $\{1, 7\}$ and 6 . Since there are only four possible input values, we can construct the Bayes-optimal classifier: w predicts $\{1, 7\}$ when u predicts 7 or when v predicts 1. The downstream test loss, ℓ_w , is the zero-one loss.

Results. Figure 4(d) shows a heat map of the downstream test loss as a function of upstream test losses. As we reduce the amount of label noise (p) from 50% down to 0%, both upstream models achieve near-zero test loss (bottom-left region). In that case, the downstream test loss also is near-optimal. When both upstream models have a high loss (top-right), the downstream model can still obtain a relatively low test loss because the upstream models only make errors when predicting classes 1 and 7. The downstream model corrects those errors. As a result, a self-defeating improvement occurs: when one upstream model improves but the other does not (top-left or bottom-right), the anti-correlated errors disappear and the downstream model can no longer separate $\{1, 7\}$ and 6 successfully.

5. Case Study: Pseudo-LiDAR for Detection

We perform a case study on self-defeating improvements in a system that may be found in self-driving cars. A second case study is presented in the supplemental material. In both cases, the system uses a pseudo-LiDAR (Wang et al., 2019) as the basis for 3D detection of cars and pedestrians. Figure 5 gives an overview of the models in the system:

- A depth-estimation model, u , takes a stereo image (a pair of rectified images from two horizontally aligned cameras) as input and predicts the depth corresponding to every pixel in the left image, creating a depth map d .
- A point cloud generator, r , uses depth map d to create a pseudo-LiDAR representation of the 3D environment.
- The stereo image and depth map are used as input into a model, v , that detects cars in the 3D environment.
- The same inputs are used in a separate model, w , that aims to perform 3D pedestrian detection.

5.1. System Design

The point cloud generator, r , is a simple non-learnable module (Wang et al., 2019). The depth-estimation and detection models used in our case study are described below.

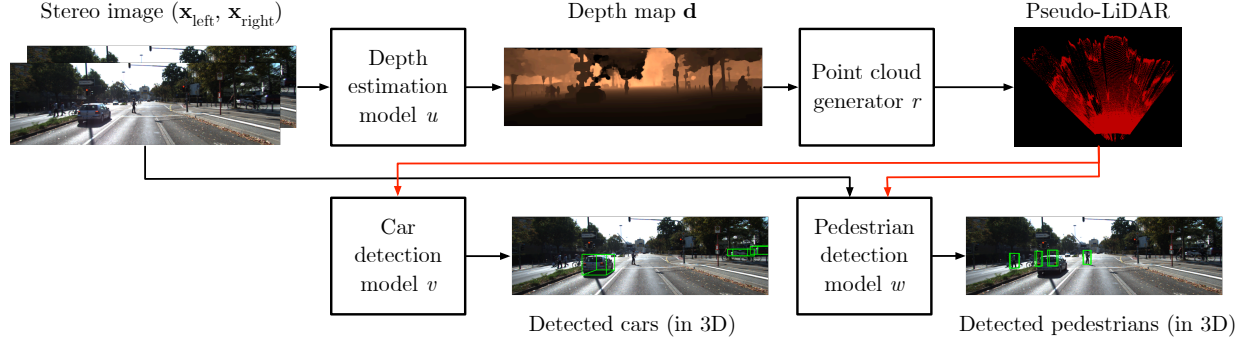


Figure 5. Overview of the car and pedestrian detection system used in our case study in Section 5. The system consists of three models: (1) a depth-estimation model u that generates a pseudo-LiDAR representation of the environment, (2) a car-detection model v that operates on 3D point clouds, and (3) a pedestrian-detection model w that performs 3D pedestrian detection.

Depth estimation. To perform depth estimation, we adopt the PSMNet model of Chang & Chen (2018). The model receives a stereo image, $(\mathbf{x}_{\text{left}}, \mathbf{x}_{\text{right}})$, as input and aims to compute a depth map, $\mathbf{d} = u(\mathbf{x}_{\text{left}}, \mathbf{x}_{\text{right}})$, that contains a depth estimate for each pixel in image \mathbf{x}_{left} . We experiment with two training loss functions: (1) the depth mean absolute error and (2) the disparity mean absolute error (MAE). Given a ground-truth depth map, \mathbf{y} , and a function that maps depths to disparities, $g(\mathbf{d}) = \frac{C}{\mathbf{d}}$, for some camera constant C , the depth MAE is proportional to $\|\mathbf{d} - \mathbf{y}\|_1$ and the disparity MAE is proportional to $\|g(\mathbf{d}) - g(\mathbf{y})\|_1$. To evaluate the quality of model u , we follow You et al. (2019) and measure depth MAE: $\ell_u(u, \bar{\mathbf{D}}_u) = \frac{1}{M} \sum_{m=1}^M \|\bar{\mathbf{d}}_m - \bar{\mathbf{y}}_m\|_1$. We expect that a model, u' , trained to minimize depth MAE will provide better depth estimates (per test loss ℓ_u) than a model, u , that is trained to minimize disparity MAE.

Car and pedestrian detection. We experiment with two different models for performing detection of cars and pedestrians, viz., the Point-RCNN model (P-RCNN; Shi et al. (2019)) and the Frustum PointNet detection model (F-PTNET; Qi et al. (2018)). Both models take stereo image $(\mathbf{x}_{\text{left}}, \mathbf{x}_{\text{right}})$ and point cloud $r(\mathbf{d})$ as input. Before computing $r(\mathbf{d})$, we perform winsorization on the prediction $u(\mathbf{x}_{\text{left}}, \mathbf{x}_{\text{right}})$: we remove all points that are higher than 1 meter in the point cloud (where the camera position is the origin). For the pedestrian-detection task, we focus on pedestrians whose distance to the camera is ≤ 20 meters by removing all points that are farther away.

Following Geiger et al. (2012), we evaluate the test loss of car-detection model, ℓ_v , using the negative average precision (AP) for an intersection-over-union (IoU) of 0.7. The test loss of the pedestrian-detection model, ℓ_w , is the negative AP for an IoU of 0.5. We measure these test losses for both the 3D box view ($-\text{AP}_{3\text{D}}$) and the 2D bird-eye view ($-\text{AP}_{\text{BEV}}$); see Geiger et al. (2012) for details on the definition of the test-loss functions.

		Car detection		Pedestrian detection	
		P-RCNN	F-PTNET	P-RCNN	F-PTNET
$\text{AP}_{3\text{D}}$	u	38.75	32.78	34.20	46.15
	u'	39.91	33.64	30.53	44.10
	y	68.06	55.46	59.08	60.99
AP_{BEV}	u	49.30	42.77	38.83	53.99
	u'	50.34	43.79	34.09	51.84
	y	78.43	67.35	64.25	65.23

Table 2. Average precision of car detection and pedestrian detection measured for 3D box view ($\text{AP}_{3\text{D}}$) and 2D birds-eye view (AP_{BEV}). Higher is better. Results are shown for baseline depth-estimation model u and an improved depth-estimation model u' that is trained using a different loss. The AP of oracle depth-estimation model y is shown for reference. Improving the depth-estimation model improves the car detection model but leads to a self-defeating improvement in the pedestrian detection model.

5.2. Experiments

We experiment with our system on the KITTI dataset (Geiger et al., 2012), using the training-validation split defined by Chen et al. (2015). Our baseline depth-estimation model, u , that is trained to minimize disparity MAE obtains a test loss of 0.820. The improved version of that model, u' , is trained to minimize depth MAE and obtains a test loss of 0.807, which confirms the model improvement.

Table 2 presents the test losses of the downstream models for car and pedestrian detection, for both the baseline upstream model u and the improved model u' . We observe that, although the improvement in depth estimation translates into an improvement in car detection, pedestrian detection suffers from a self-defeating improvement: the $\text{AP}_{3\text{D}}$ drops from 46.15 to 44.10 (from 53.99 to 51.84 in AP_{BEV}) when the depth-estimation model is improved.

The self-defeating improvement observed in Table 2 likely belongs to the test-loss mismatch category of entanglement

Range	0-max	0-10	10-20	20-30	30-40	40-max
Model u	0.820	0.237	0.476	1.327	2.346	4.566
Model u'	0.807	0.270	0.491	1.289	2.240	4.205

Table 3. Depth MAE test loss of depth-estimation models u (trained to minimize disparity MAE) and u' (trained to minimize depth MAE), split out per range of ground-truth depth values (columns; in meters). Model u predicts the depth of nearby points more accurately, but model u' works better on distant points.

between upstream and downstream. A depth-estimation model that is trained to minimize disparity MAE (*i.e.*, model u) focuses on making sure that *small* depth values (large disparity values) are predicted correctly. By contrast, a model trained to minimize depth MAE (model u') concentrates on predicting *large* depth values correctly; see Table 3 for details. This is beneficial for the car-detection task because most cars tend to be relatively far away. However, it negatively affects the pedestrian detector because that detector only needs to detect nearby pedestrians (with a distance ≤ 20 meters to the stereo camera). In other words, the loss function that improves model u deteriorates the downstream performance because it focuses on errors that are less relevant to the downstream model.

6. Related Work

This study is part of a larger body of work around *machine-learning engineering*² (Burkov, 2020; Lwakatarea et al., 2020; Ozkaya, 2020). Sculley et al. (2015) provides a good overview of the types of problems that machine-learning engineering is concerned with. The setting studied in this paper is an example of the entanglement problem (Amershi et al., 2019; Nushi et al., 2017), where “changing anything changes everything” (Sculley et al., 2015). Entanglement is the main underlying cause of the self-defeating improvements we study in this paper. Issues due to entanglement can be further exacerbated by having humans-in-the-loop during learning; a situation that commonly arises, for example, in computational advertising (Bottou et al., 2013).

Several aspects of self-defeating improvements have been studied extensively elsewhere in the literature. In particular, the effect of a change in an upstream model on a downstream model can be viewed as a variant of *domain shift* (see, *e.g.*, Ben-David et al. (2010); Patel et al. (2015)). However, common approaches to domain shift, such as importance weighting of training examples (Shimodaira, 2000), may not be directly applicable because they require the input data space of both models to be identical.

The study of self-defeating improvements is also related to

²See <https://github.com/visenger/awesome-mlops> for a large set of resources about machine learning engineering.

the study of *transfer learning* (*e.g.*, Azizpour et al. (2016); Kornblith et al. (2019); Pan & Yang (2010)). Prior work on transfer learning has reported examples of self-defeating improvements: for example, Kornblith et al. (2019) report that some regularization techniques improve the accuracy of convolutional networks on ImageNet, but negatively affect the transfer of those networks to other recognition tasks. This paper extends prior studies on transfer learning by studying downstream effects of model *updates*.

Finally, work on *differentiable programming* (Innes et al., 2019; Wang et al., 2018) is relevant to the study of self-defeating improvements. In some situations, a self-defeating improvement may be resolved by backpropagating learning signals from a model further upstream. However, such an approach is not a panacea as downstream tasks may have conflicting goals (see Section 5). Moreover, technical or practical obstacles may prevent the use of differentiable programming in practice (see Section 2).

7. Conclusion and Future Work

This study explored self-defeating improvements in modular machine-learning systems. In particular, we demonstrated how different types of entanglement between machine-learning models can give rise to self-defeating improvements. The findings presented in this study suggest a plethora of directions for future work:

- Our study focused on *first-order* entanglement between two models (either an upstream and a downstream model or two upstream models). Some settings may give rise to higher-order entanglements, for example, between three upstream models whose errors cancel each other out.
- Our definition of different types of entanglement may pave the way for the development of *diagnostic tools* that identify the root cause of a self-defeating improvement.
- It would also be useful to develop *best practices* that can help prevent self-defeating improvements from occurring. One way to do so may be by tightening the “API” of the machine-learning models, for example, by calibrating classifier outputs (Guo et al., 2017) or whitening feature representations (Krizhevsky & Hinton, 2009). Such transforms constrain the output distribution of the model, which may reduce the negative effects of model changes on their downstream dependencies.
- Further work is also needed into self-defeating improvements of aspects such as model fairness. Indeed, an important open question is: *Can making an upstream model fairer make its downstream dependencies less fair?*

We hope this paper will foster the study of such machine-learning systems engineering questions, and will inspire the machine-learning community to rigorously study machine-learning systems in addition to individual models.

Acknowledgements

The authors thank Yan Wang, Yurong You, and Ari Morcos for helpful discussions and advice.

References

- Amershi, S., Begel, A., Bird, C., DeLine, R., Gall, H., Kamar, E., Nagappan, N., Nushi, B., and Zimmermann, T. Software engineering for machine learning: A case study. In *Proceedings of the International Conference on Software Engineering*, 2019.
- Arazo, E., Ortego, D., Albert, P., O'Connor, N. E., and McGuinness, K. Unsupervised label noise modeling and loss correction. *arXiv preprint arXiv:1904.11238*, 2019.
- Azizpour, H., Razavian, A. S., Sullivan, J., Maki, A., and Carlsson, S. Factors of transferability for a generic convnet representation. *IEEE Trans. Pattern Anal. Mach. Intell.*, 38(9):1790–1802, 2016.
- Ben-David, S., Blitzer, J., Crammer, K., Kulesza, A., Pereira, F., and Vaughan, J. W. A theory of learning from different domains. *Machine Learning*, 79:151–175, 2010.
- Bottou, L., Peters, J., Quinero-Candela, J., Charles, D. X., Chikering, D. M., Portugaly, E., Ray, D., Simard, P., and Snelson, E. Counterfactual reasoning and learning systems: The example of computational advertising. *Journal of Machine Learning Research*, 14:3207–3260, 2013.
- Brown, T. B., Mann, B., Ryder, N., Subbiah, M., Kaplan, J. D., Dhariwal, P., Neelakantan, A., Shyam, P., Sastry, G., Askell, A., Agarwal, S., Herbert-Voss, A., Krueger, G. M., Henighan, T., Child, R., Ramesh, A., Ziegler, D., Wu, J., Winter, C., Hesse, C., Chen, M., Sigler, E., Litwin, M., Gray, S., Chess, B., Clark, J., Berner, C., McCandlish, S., Radford, A., Sutskever, I., and Amodei, D. Language models are few-shot learners. In *Advances in Neural Information Processing*, 2020.
- Burkov, A. *Machine Learning Engineering*. True Positive Inc., 2020.
- Caruana, R. Multi-task learning. *Machine Learning*, 28: 41–75, 1997.
- Chang, J.-R. and Chen, Y.-S. Pyramid stereo matching network. In *Proceedings of the IEEE Conference on Computer Vision and Pattern Recognition*, pp. 5410–5418, 2018.
- Chen, X., Kundu, K., Zhu, Y., Berneshawi, A. G., Ma, H., Fidler, S., and Urtasun, R. 3d object proposals for accurate object class detection. In *Advances in Neural Information Processing Systems*, pp. 424–432. Citeseer, 2015.
- D’Amour, A., Heller, K., Moldovan, D., Adlam, B., Alipanahi, B., Beutel, A., Chen, C., Deaton, J., Eisenstein, J., Hoffman, M. D., Hormozdiari, F., Houlisby, N., Hou, S., Jerfel, G., Karthikesalingam, A., Lucic, M., Ma, Y., McLean, C., Mincu, D., Mitani, A., Montanari, A., Nado, Z., Natarajan, V., Nielson, C., Osborne, T. F., Raman, R., Ramasamy, K., Sayres, R., Schrouff, J., Seneviratne, M., Sequeira, S., Suresh, H., Veitch, V., Vladymyrov, M., Wang, X., Webster, K., Yadlowsky, S., Yun, T., Zhai, X., and Sculley, D. Underspecification presents challenges for credibility in modern machine learning. In *arXiv:2011.03395*, 2020.
- Geiger, A., Lenz, P., and Urtasun, R. Are we ready for autonomous driving? The KITTI vision benchmark suite. In *Proceedings of the IEEE Conference on Computer Vision and Pattern Recognition*, 2012.
- Glenn Brookshear, J. *Computer Science. An Overview (9th edition)*. Addison-Wesley, 2009.
- Guo, C., Pleiss, G., and Weinberger, Y. S. K. Q. On calibration of modern neural networks. In *Proceedings of the International Conference on Machine Learning*, pp. 1321–1330, 2017.
- Hamming, R. W. *The Art of Doing Science and Engineering*. Gordon and Breach Science Publishers, 1997.
- He, K., Zhang, X., Ren, S., and Sun, J. Deep residual learning for image recognition. In *Proceedings of the IEEE Conference on Computer Vision and Pattern Recognition*, pp. 770–778, 2016.
- Innes, M., Edelman, A., Fischer, K., Rackauckas, C., Saba, E., Shah, V., and Tebbutt, W. A differentiable programming system to bridge machine learning and scientific computing. In *arXiv:1907.07587*, 2019.
- Kingma, D. and Ba, J. Adam: A method for stochastic optimization. In *Proceedings of the International Conference on Learning Representations*, 2014.
- Kornblith, S., Shlens, J., and Le, Q. V. Do better ImageNet models transfer better? In *Proceedings of the IEEE Conference on Computer Vision and Pattern Recognition*, pp. 2661–2671, 2019.
- Krizhevsky, A. and Hinton, G. Learning multiple layers of features from tiny images. Technical report, University of Toronto, 2009.
- Lwakatarea, L., Raj, A., Crnkovic, I., Bosch, J., and Olsson, H. H. Large-scale machine learning systems in real-world industrial settings: A review of challenges and

- solutions. *Information and Software Technology*, 127, 2020.
- Netzer, Y., Wang, T., Coates, A., Bissacco, A., Wu, B., and Ng, A. Y. Reading digits in natural images with unsupervised feature learning. In *NeurIPS Workshop on Deep Learning and Unsupervised Feature Learning*, 2011.
- Nushi, B., Kamar, E., Horvitz, E., and Kossmann, D. On human intellect and machine failures: Troubleshooting integrative machine learning systems. In *Proceedings of AAAI Conference on Artificial Intelligence*, 2017.
- Ozkaya, I. What is really different in engineering ai-enabled systems? *IEEE Software*, 37(4), 2020.
- Pan, S. J. and Yang, Q. A survey on transfer learning. *IEEE Transactions on Knowledge and Data Engineering*, 22: 1345–1359, 2010.
- Patel, V. M., Gopalan, R., Li, R., and Chellappa, R. Visual domain adaptation: A survey of recent advances. *IEEE Signal Processing Magazine*, 32:53–69, 2015.
- Qi, C. R., Liu, W., Wu, C., Su, H., and Guibas, L. J. Frustum pointnets for 3D object detection from RGB-D data. In *Proceedings of the IEEE Conference on Computer Vision and Pattern Recognition*, pp. 918–927, 2018.
- Sculley, D., Holt, G., Golovin, D., Davydov, E., Phillips, T., Ebner, D., Chaudhary, V., Young, M., Crespo, J.-F., and Dennison, D. Hidden technical debt in machine learning systems. In *Advances in Neural Information Processing Systems*, 2015.
- Shi, S., Wang, X., and Li, H. PointRCNN: 3D object proposal generation and detection from point cloud. In *Proceedings of the IEEE Conference on Computer Vision and Pattern Recognition*, pp. 770–779, 2019.
- Shimodaira, H. Improving predictive inference under covariate shift by weighting the log-likelihood function. *Journal of Statistical Planning and Inference*, 90:227–244, 2000.
- Wang, F., Decker, J., Wu, X., Essertel, G., and Rompf, T. Backpropagation with callbacks: Foundations for efficient and expressive differentiable programming. In *Advances in Neural Information Processing Systems*, volume 31, 2018.
- Wang, Y., Chao, W.-L., Garg, D., Hariharan, B., Campbell, M., and Weinberger, K. Q. Pseudo-LiDAR from visual depth estimation: Bridging the gap in 3D object detection for autonomous driving. In *Proceedings of the IEEE Conference on Computer Vision and Pattern Recognition*, pp. 8445–8453, 2019.
- You, Y., Wang, Y., Chao, W.-L., Garg, D., Pleiss, G., Hariharan, B., Campbell, M., and Weinberger, K. Q. Pseudo-LiDAR++: Accurate depth for 3D object detection in autonomous driving. *arXiv preprint arXiv:1906.06310*, 2019.

Supplementary Material

Fixes That Fail: Self-Defeating Improvements in Machine-Learning Systems

A. Case Study II:

Pseudo-LiDAR for Detection

In this section, we present a second case study of self-defeating improvements that may arise in 3D detection based on pseudo-LiDAR. In contrast to the case study in Section 5 in which the self-defeating improvement was caused by loss mismatch, this case centers on data-distribution mismatch. We adopt a very similar setup as in Section 5 but, here, we focus exclusively on the detection of pedestrians whose distance to the camera is ≤ 20 meters.

A.1. System Design

We describe the depth-estimation and detection models we used in our case study separately below.

Depth estimation. As before, we adopt the PSMNet model of Chang & Chen (2018) for depth estimation. The model receives a stereo image, $(\mathbf{x}_{\text{left}}, \mathbf{x}_{\text{right}})$, as input and predicts a depth map, $\mathbf{d} = u(\mathbf{x}_{\text{left}}, \mathbf{x}_{\text{right}})$, that contains a depth estimate for each pixel in image \mathbf{x}_{left} . However, we swap the upstream models u and u' compared to Section 5.1 to better match the downstream task (pedestrian detection). For the same reason, we also change the test-loss function.

In Section 5.2, we discussed the difference between disparity MAE and depth MAE: a model trained to minimize depth MAE concentrates on predicting *large* depth values correctly, but a depth-estimation model that is trained to minimize disparity MAE focuses on making sure that *small* depth values (large disparity values) are predicted correctly. Since this case study focuses on detection of pedestrians ≤ 20 meters away as downstream task, adopt disparity MAE as the upstream test-loss function. Hence, the test-loss function is: $\ell_u(u, \mathcal{D}_u) = \frac{1}{M} \sum_{m=1}^M \|g(\hat{\mathbf{d}}_m) - g(\tilde{\mathbf{y}}_m)\|_1$, where g transforms depth values into disparity values. We train the baseline upstream model, u , to minimize depth MAE. The improved upstream model, u' , is trained to minimize disparity MAE instead.

Pedestrian detection. Figure S1 illustrates the system we study. We use the same 3D pedestrian-detection models as before, *viz.*, P-RCNN and F-PTNET. However, we alter the way in which the models are used compared to Section 5.1. The key difference compared to Section 5.1 is that the 3D pedestrian detection model receives non-winsorized pseudo-LiDAR representations, and is trained to detect pedestrians at any distance. Pedestrian detections that are farther away than 20 meters are removed post-hoc.

		P-RCNN	F-PTNET
AP _{3D}	u	34.42	43.02
	u'	27.64	43.10
	y	55.19	62.16
AP _{BEV}	u	38.51	50.49
	u'	31.47	48.29
	y	63.00	65.92

Table S1. Average precision at IoU 0.5 of pedestrian detection measured for 3D box view (AP_{3D}) and 2D birds-eye view (AP_{BEV}) for two different detection models (P-RCNN and F-PTNET). Results are shown for the baseline depth-estimation model, u , the improved depth-estimation model, u' , and an oracle depth-estimation model, y . Higher is better.

To evaluate the downstream models, we use the same downstream test-loss function as in Section 5: we measure the AP at IoU 0.5 of detection of pedestrians ≤ 20 meters from the camera for both the 3D box view ($-\text{AP}_{3D}$) and the 2D bird-eye view ($-\text{AP}_{BEV}$).

A.2. Experiments

As before, we experiment on the KITTI dataset (Geiger et al., 2012) using the same setup as in Section 5. The baseline depth-estimation model, u , that is trained to minimize depth MAE obtains an upstream test loss of 1.277. The improved version of that model, u' , is trained to minimize disparity MAE and obtains a test loss of 1.207, which confirms the upstream model improvement.

Table S1 presents the test losses of the downstream models for pedestrian detection, for both the baseline upstream model u and the improved model u' . For reference, we also present the downstream test-loss for an oracle upstream model, y . From the results in the table, we observe that a self-defeating improvement arises. In particular, the P-RCNN model’s AP_{3D} decreases from 34.42 to 27.64 (from 38.51 to 31.47 in AP_{BEV}) when the upstream model is improved. For the F-PTNET, the self-defeating improvement is less pronounced but the effect of the upstream improvement on the downstream model does appear to be negative.

We hypothesize that this self-defeating improvement is caused by a loss-function mismatch. Intuitively, the detection models learn to recognize the shape of pedestrians in 3D cloud points. Revisiting Table 3, we observe that depth-estimation model u' (denoted by u in Table 3) makes larger

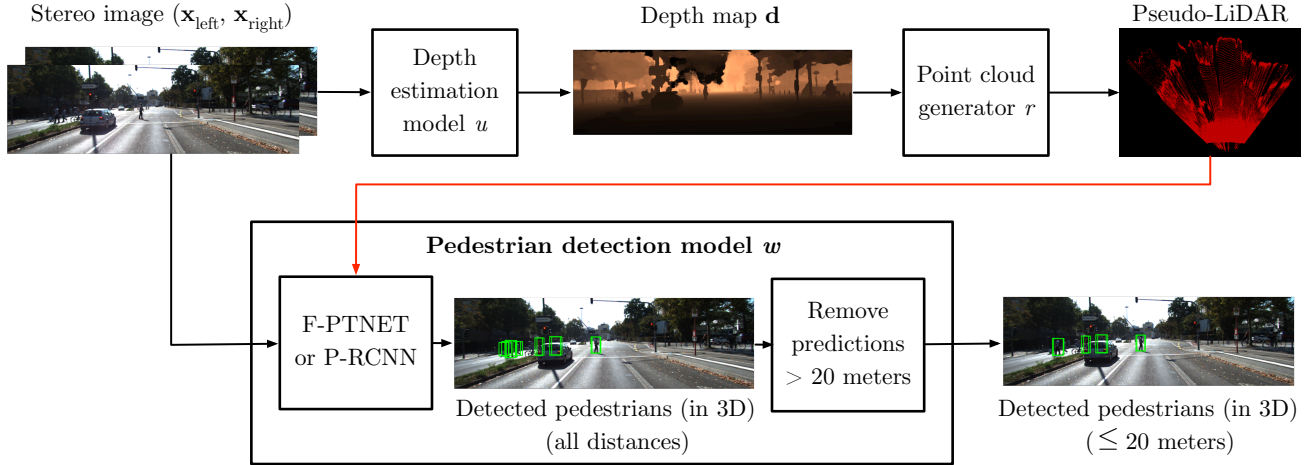


Figure S1. Overview of the pedestrian detection system used in our case study in Appendix A. The 3D pedestrian detection model in we focus on here receives a non-winsorized pseudo-LiDAR point cloud as input, and is trained to detect pedestrians across the full range of distances. Pruning of detection boxes that are farther away than 20 meters only happens post-hoc.

errors than depth-estimation model u (denoted by u' in the table) for distant points. Hence, the point representations produced by model u' are much noisier for far-away pedestrians than those produced by u . Because the downstream model is trained to detect these far-away pedestrians, the noise in the pedestrian point clouds makes it harder for that model to learn a good model of the shape of pedestrians. This results in the self-defeating improvement.

B. Details on Experimental Setup

In this section, we present details on the setup of the experiments presented in Section 4. Specifically, we present details on the model training, model selection, and definition of the test loss-function. Code reproducing our experiments is available in the supplemental material.

Model training. We provide details on model architecture, training loss function, and optimizer:

- **Model architecture.** The model architectures we used in our experiments are presented in Table 1. The convolutional network that we used in the experiment studying hypothesis-space mismatch consists of two convolutional layers with 32 channels and one fully connected layer. In both convolutional layers, we set the kernel size to 5. The stride of the first layer is 1; the second layer’s stride is 2. The number of padded zeros is set to 2 and 5, respectively. After each convolutional layer, batch normalization is applied and a rectified linear unit (ReLU) activation function is computed.
- **Training loss function.** In all classification tasks, we adopted the cross-entropy (logistic) loss function for training. For the regression task in the loss-function mis-

match experiment, the training loss function is the mean squared error (MSE) loss. We do not regularize the loss, but we do apply random cropping and horizontal flipping (Krizhevsky & Hinton, 2009) on the SVHN images when training the upstream models.

- **Optimizer.** Optimization of the training loss with respect to the parameters is performed using the Adam optimizer (Kingma & Ba, 2014). We performed 200 training epochs for all upstream classification models, 500 epochs for the upstream regression model, and 100 epochs for all downstream models. We set the initial learning rate to 0.001 when training upstream models, and to 0.01 when training downstream models. We decay the learning rate by a factor of 10 halfway training, and again after three-quarter of the training epochs.

Model selection. The classification models we trained did not overfit; hence, we simply use the model obtained after the training has completed. The regression model (in the loss-function mismatch experiment) is prone to overfitting, so we used early stopping: we select the best model among the models obtained after each training epoch.

Test loss function. Table 1 lists the loss functions we used to measure the quality of our models on the test set. In most experiments, we simply evaluated the zero-one loss (*i.e.*, classification error) or the mean squared error (MSE). To assess the quality of feature representations, we used a nearest-neighbor loss function. To compute this loss, we split the test set into two non-overlapping subsets that contain the same number of examples. We predict the labels of the examples in the second subset using a one-nearest-neighbor classifier “trained” on the subset. We report the classification error of the resulting predictions.